Big Data and Information Analytics

BDIA, 10: 70–80.
DOI: 10.3934/bdia.2026004
Received: 22 November 2025
Revised: 08 December 2025
Accepted: 10 December 2025
Published: 02 March 2026

https://www.aimspress.com/journal/BDIA

Research article

Degradation-mediated adsorption of BMP-2 on magnesium surfaces

Yu Zhao[1,2,*]

[1] State Key Lab of Metal Matrix Composites, School of Materials Science and Engineering, Shanghai Jiao Tong University, Shanghai 200240, China
[2] School of Materials Science and Engineering, Zhengzhou University, Zhengzhou 450001, China

* **Correspondence:** Email: zy0805@sjtu.edu.cn.

Abstract: Bone defect repair remains a major challenge in current orthopedic surgery. Autologous or allogeneic bone grafting and metallic fixation are widely-used clinical approaches, but their effectiveness is limited by insufficient donor sources and immunological risks. To overcome these limitations, bone tissue engineering has been developed to regenerate functional bone based on an improved understanding of bone structure and bone formation. Among various osteogenic factors, bone morphogenetic protein-2 (BMP-2) plays a pivotal role in promoting new bone formation at defect sites and is therefore central to the design of biomaterial-assisted bone tissue engineering strategies. In this study, the influence of pure magnesium (Mg) degradation and different degradation degrees on the adsorption behavior of BMP-2 was systematically investigated. The combined results of BMP-2 adsorption experiments and molecular dynamics simulations demonstrate that degradation of Mg reduces the number of BMP-2 adsorption sites on the surface and progressively weakens the interfacial interaction strength as degradation proceeds. This effect is attributed to degradation-induced charge redistribution on the Mg surface, which leads to a reorganization of the interfacial hydrated layer and ultimately inhibits BMP-2 adsorption on Mg.

Keywords: magnesium; molecular dynamics simulation; BMP-2

1. Introduction

Bone defects are challenging clinical conditions in orthopedic practice, most commonly caused by trauma, infection, and tumors [1,2]. Compared with implants that merely fill the defect volume with biologically inert materials, bone tissue engineering aims to repair bone defects by using bioactive

materials to regenerate functional bone tissue, based on an in depth understanding of bone biology and structure [3,4]. Bioactive materials for bone tissue engineering are therefore required to provide both mechanical support and stimulation of bone regeneration. In recent years, magnesium (Mg) has emerged as a promising orthopedic metal due to its good biocompatibility and biodegradability, as well as an elastic modulus close to that of natural cortical bone [5–7]. Accumulating evidence indicates that Mg ions released from Mg implants are essential trace elements for the human body and can stimulate the activity of bone progenitor cells [8], thereby accelerating the formation of new bone tissue and blood vessels. In addition, Mg exhibits antibacterial and anti-tumor properties that are uncommon among currently used clinical bone repair materials, further supporting its potential as a new generation of bone repair implants [9]. However, the rapid and non-uniform degradation and severe localized corrosion of Mg significantly limit its application in medical implantation.

In general, three key components are involved in bone tissue engineering: scaffolds, growth factors, and cells [10–12]. Bone healing is regulated by multiple growth factors, including bone morphogenetic proteins (BMPs), transforming growth factor β (TGF-β), fibroblast growth factors, and vascular endothelial growth factors, among others [13]. BMPs are secreted by various cell types, such as endothelial cells, osteoblasts, and chondrocytes, and activate downstream signaling pathways by binding to specific transmembrane receptors. Bone morphogenetic protein 2 (BMP-2), one member of this family, was approved by the US Food and Drug Administration (FDA) in 2002 for use in bone regenerative systems [14]. By regulating the differentiation of osteoblasts and osteoclasts, BMP-2 modulates the balance between bone formation and resorption and is widely regarded as a promising growth factor for bone tissue engineering.

A central challenge in the design of bone tissue engineering constructs is the effective delivery of functional biochemical signaling molecules, such as BMP-2, to bone defect sites via suitable carriers in order to promote bone tissue regeneration [15]. For Mg-based bone tissue engineering materials, in addition to appropriate mechanical properties and degradability, a sufficient loading capacity for BMP-2 is required to ensure sustained bioactivity and to accelerate osteogenic differentiation at fracture sites. Kim et al. reported that immobilizing BMP-2 on a layer-by-layer (LBL) carrier consisting of micro-arc oxidation (MAO) coating and hydrothermal treatment could slow the degradation rate of Mg alloys in vivo and enhance bone formation through sustained BMP-2 release [16]. Characterizing the changes in BMP-2 adsorption strength on Mg surfaces with different degrees of hydroxylation can directly reveal how Mg degradation influences BMP-2 loading capacity, which is an important criterion for evaluating the feasibility of Mg as a bone tissue engineering material.

Therefore, a detailed understanding of the kinetics and thermodynamics of BMP-2 adsorption on Mg surfaces with varying hydroxylation degrees is of great importance. In this study, the adsorption behavior of BMP-2 on Mg surfaces with different degradation degrees was investigated by combining molecular dynamics (MD) simulations with fluorescence BMP-2 adsorption experiments. The results show that Mg degradation inhibits BMP-2 adsorption, and the adsorption capacity decreases progressively with increasing degradation degree. Analysis of the adsorption structures and energies indicates that two oppositely oriented hydration layers form on Mg surfaces, and degradation-induced charge redistribution on the Mg surface leads to reorientation of interfacial water molecules, which is the primary reason for the weakened BMP-2 adsorption. This work takes the effect of Mg degradation on BMP-2 adsorption as the starting point and provides a scientific basis for the feasibility design of Mg-based materials for bone tissue engineering.

2. Computational and experimental methods

2.1. Models and MD simulations

The initial configuration of BMP-2 was obtained from the RCSB Protein Data Bank (PDB ID: 3BMP). In the early degradation stage of Mg in an aqueous environment, the main corrosion product on the Mg surface was Mg hydroxide. To represent Mg surfaces at different degradation stages, model surfaces uniformly decorated with different numbers of hydroxyl pairs were constructed. Mg surfaces with hydroxyl coverages of 0, 10%, 20%, 50%, and 100% were denoted as Mg, MgOH1, MgOH2, MgOH5, and MgOH15, respectively, and the corresponding structural units were optimized using density functional theory. On the basis of preliminary tests, the use of a fixed Mg substrate was found to have only a minor influence on the adsorption behavior of biomolecules; therefore, all Mg atoms in the slab were kept fixed throughout the simulations.

MD simulations were performed using GROMACS version 5.1.4. The simulation cell was a rectangular box with dimensions of 60.8 × 63.5 × 87.3 Å^3. The Mg substrate was placed at the bottom of the box, and the solution phase was placed above it. The Mg substrate was generated by cleaving the Mg crystal along the direction with a thickness of four atomic layers. The neutral aqueous environment consisted of one BMP-2 molecule, approximately 50000 water molecules, and Na^+ or Cl^- counterions, with the BMP-2 molecule initially positioned 60 Å above the Mg surface. The interaction between BMP-2 and Mg was described using a modified Lennard-Jones (LJ) nonbonded force field reported and validated by Zhen et al. [17]. The systems were modeled using the Amber14SB force field for BMP-2 and ions [18], and the TIP3P model for water molecules [19, 20]. Electrostatic interactions were treated with the particle-mesh Ewald (PME) method [21], using a real-space cutoff of 14 Å, and LJ nonbonded interactions were smoothly switched to zero as the interatomic distance approached 14 Å. All simulations were performed with a time step of 1.5 fs under three-dimensional periodic boundary conditions. Initially, each system was relaxed for 600 ps in the NVT ensemble at 300 K using the V-rescale thermostat, followed by 600 ps of equilibration in the NPT ensemble at 1 bar. Finally, production runs of 100 ns at 300 K were carried out to obtain the adsorbed configurations, which were subsequently analyzed for structural characteristics and adsorption energies.

2.2. Alkali heat treatment and fluorescence measurements

The degradation products of Mg in aqueous solution are mainly composed of Mg hydroxide. In this study, Mg samples with different degradation degrees were prepared by alkaline heat treatment. Mg plates with dimensions of 10 mm × 10 mm × 2 mm were sequentially ground with 200#, 400#, 600#, and 800# metallographic abrasive papers, ultrasonically cleaned in ethanol for 5 min, and then dried with hot air. The cleaned Mg samples were subsequently immersed in 3 mol/L NaOH solution at 80 °C for 30 min, 3 h, and 6 h, and were designated as MgOH-1, MgOH-2, and MgOH-3, respectively. A longer alkaline heat-treatment time resulted in a higher surface hydroxyl coverage; therefore, Mg, MgOH-1, MgOH-2, and MgOH-3 represent Mg surfaces with progressively increasing degradation degrees.

A stock solution of BMP-2 labeled with fluorescein isothiocyanate (FITC-BMP-2, 0.22 mg/mL) was diluted with deionized water to a final concentration of 15 μg/mL. Mg, MgOH-1, MgOH-2, and MgOH-3 samples were immersed in the FITC-BMP-2 solution (15 μg/mL) for 20, 40, and 60 min,

respectively. The adsorbed FITC-BMP-2 on the Mg surfaces was observed using a fluorescence microscope (Nikon Eclipse Ts100, Japan). To ensure experimental reproducibility, three duplicate samples were prepared for each condition (Mg, MgOH-1, MgOH-2, and MgOH-3), and FITC-BMP-2 adsorption was evaluated for each sample. For quantitative analysis, the number of FITC-BMP-2 bright spots was counted in at least three randomly selected regions per sample, and the adhesion protein number density was defined as the number of adherent proteins divided by the corresponding image area.

3. Results and discussion

3.1. Understanding the BMP-2 adsorption behavior with experiments

The amount of BMP-2 adsorbed on different Mg surfaces reflects their BMP-2 loading capacity, that is, Mg degradation modulates protein adsorption. FITC-BMP-2 adsorption on the surfaces of Mg, MgOH-1, MgOH-2, and MgOH-3 at different immersion times is shown in Figure 1, and the corresponding number density of adherent FITC-BMP-2 is presented in Figure 2. The undegraded Mg surface exhibits the fastest BMP-2 adsorption; compared with 20 min, the amount of BMP-2 on Mg reaches its maximum at 40 min, while pronounced corrosion pits appear on the Mg surface after 60 min of immersion. Relative to Mg, the amount of BMP-2 adsorbed on MgOH-1 is markedly reduced, and further decreases are observed on MgOH-2 and MgOH-3 as the degree of surface hydroxylation increases. These results indicate that Mg degradation progressively inhibits BMP-2 adsorption on the surface. BMP-2 can recruit undifferentiated mesenchymal stem cells (MSCs) to bone defect sites and subsequently activate the BMP signaling pathway.

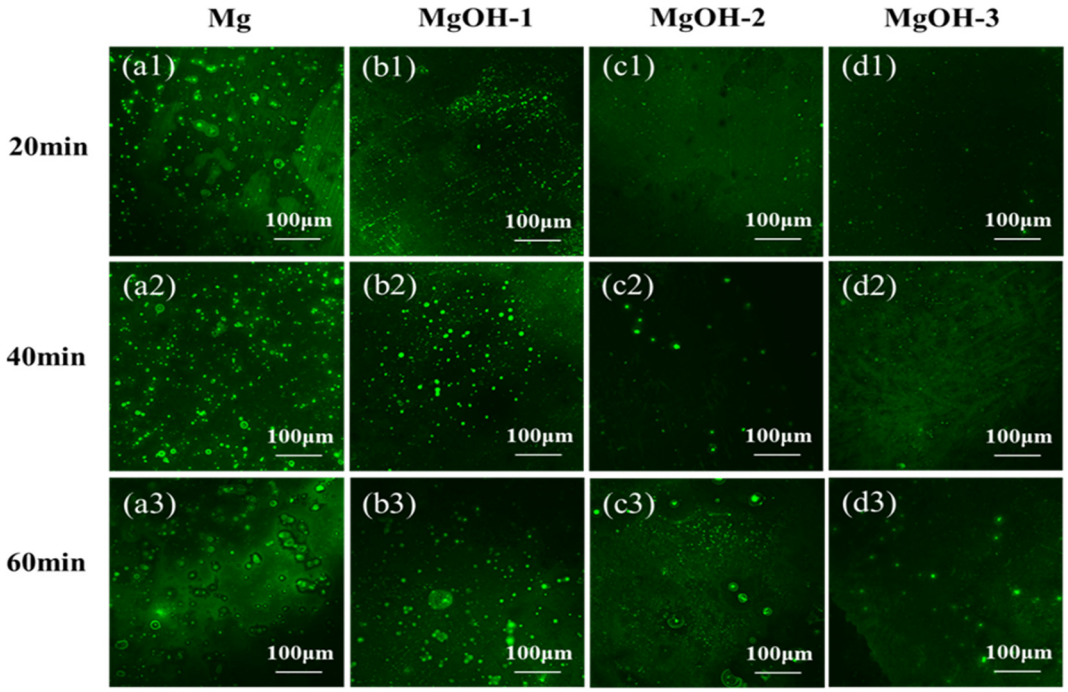

Figure 1. Adsorption imags of FITC-BMP2 on Mg, MgOH-1, MgOH-2, MgOH-3 samples after immersion 20 min, 40 min, and 60 min.

Therefore, elucidating the adsorption mechanism of BMP-2 at the atomic level in aqueous environments is essential for optimizing the design of Mg-based scaffolds to enhance biological responses and regulate the degradation behavior of Mg.

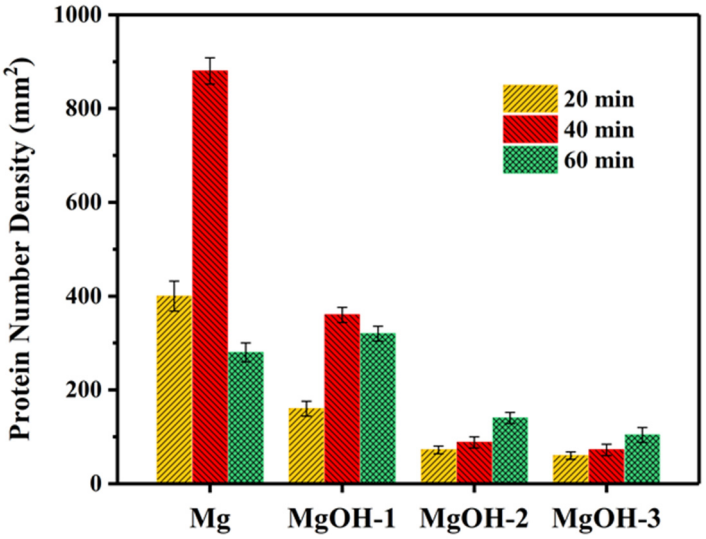

Figure 2. Average number density of FITC-BMP2 adsorbed on Mg, MgOH-1, MgOH-2, MgOH-3 surfaces.

3.2. BMP-2 adsorption behavior with MD simulations

Direct experimental observation of the detailed protein adsorption process and the associated interaction forces is extremely difficult. Therefore, MD simulations were employed to investigate the adsorption behavior of BMP-2 on Mg surfaces with different degrees of hydroxylation and to elucidate the molecular mechanism by which Mg degradation influences BMP-2 adsorption [22]. To more intuitively capture the effect of degradation degree, Mg surfaces with hydroxyl coverages of 0, 10%, 20%, 50%, and 100% were constructed and denoted as Mg, MgOH1, MgOH2, MgOH5, and MgOH15, respectively.

The adsorption energy provides a direct measure of the BMP-2 adsorption capacity on Mg surfaces. Figure 3(a) shows the evolution of the total adsorption energy between BMP-2 and the different surfaces during the MD simulations. The interaction strength follows the order Mg > MgOH1 > MgOH2 > MgOH15 > MgOH5, indicating that BMP-2 adsorption is strongest on the undegraded Mg surface. Upon surface hydroxylation, the adsorption strength of BMP-2 gradually decreases as the number of hydroxyl groups increases. In the simulations, the interaction energy between BMP-2 and the Mg surfaces consists of van der Waals and electrostatic contributions, as summarized in Figure 3(b). During the diffusion and adsorption of BMP-2, the adsorption on Mg, MgOH1, MgOH2, and MgOH15 is predominantly governed by van der Waals interactions, which decrease with increasing hydroxyl coverage, whereas the electrostatic interaction component progressively increases as more hydroxyl groups are present on the surface.

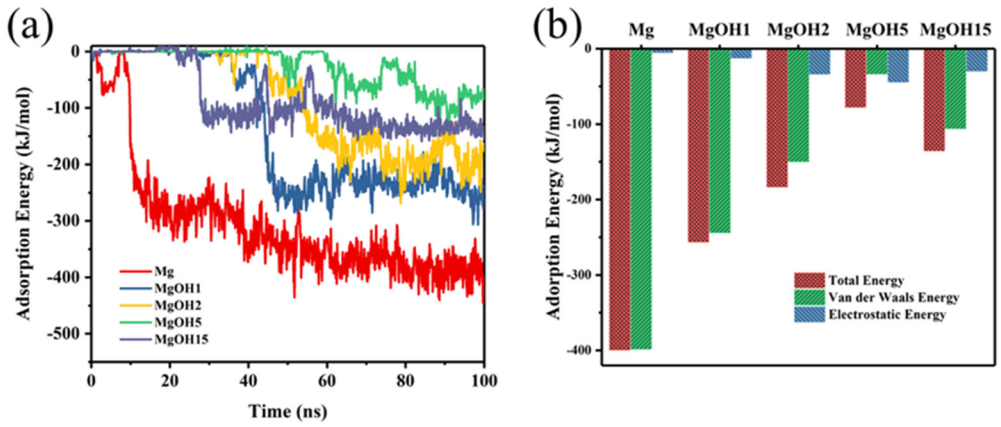

Figure 3. The interaction energy between BMP-2 and Mg, MgOH1, MgOH2, MgOH5 and MgOH15 during the MD simulations. (a) Total adsorption energy and (b) average value of total energy, van der Waals energy, and electrostatic energy at final 20 ns.

To characterize the diffusion and adsorption process of BMP-2 on the Mg surfaces in more detail, the contact surface area (CSA) between BMP-2 and the substrate, as well as the distance between their centers of mass, were calculated over the course of the MD simulations. As shown in Figure 4(a),(b), BMP-2 reaches a stable adsorption state after an initial period of fluctuation upon first contacting the substrate. The CSA and center-of-mass distance between BMP-2 and the Mg surfaces provide quantitative descriptors of the adsorption configuration of the protein on each substrate.

After approximately 60 ns of MD simulation, both the CSA and the center-of-mass distance between BMP-2 and all five surfaces converge to stable values. BMP-2 on the Mg surface exhibits the largest CSA and the smallest center-of-mass distance, indicating the greatest degree of spreading and the closest approach of the protein to the substrate. Consistent with the trend in adsorption energy, the CSA of BMP-2 on MgOH1/MgOH5 decreases progressively, while the center-of-mass distance increases correspondingly, further confirming that Mg degradation inhibits BMP-2 adsorption on the surface by reducing interfacial contact.

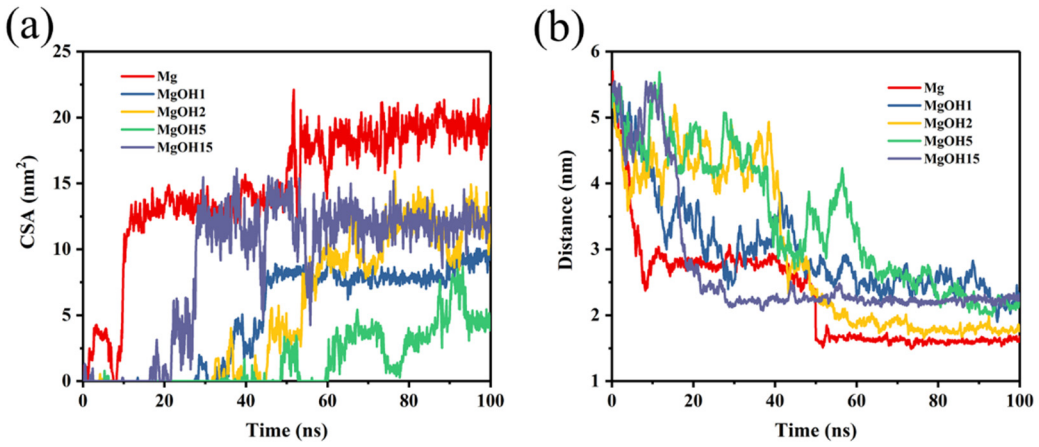

Figure 4. (a) Contact surface area (CSA) and (b) distance between BMP-2 and Mg, MgOH1, MgOH2, MgOH5 and MgOH15 during the MD simulations.

After 100 ns of MD simulation, the stable adsorption configurations of BMP-2 on the five Mg surfaces and the corresponding "anchoring" residues are summarized in Figure 5 and Table 1. The number and spatial distribution of these residues reflect the extent of BMP-2 spreading on each surface. When BMP-2 is adsorbed on Mg (Figure 5(a)), the residues in direct contact with the surface are mainly located in the α-helix region of the active site (PHE51-VAL67) and in the GLU86-ASN87 segment at the opposite end of the protein. In this case, a total of 19 residues are anchored on the Mg surface, distributed at both termini of the protein, effectively "fixing" BMP-2 onto the substrate.

Upon degradation of Mg, the anchoring pattern changes markedly. On MgOH1, the anchoring residues are primarily located in the VAL25-PRO27 and GLU88-VAL91 regions (Figure 5(b)), and their total number decreases to seven. With further increase in degradation degree, the number of BMP-2 residues anchored on MgOH2 is reduced to only three, namely ASN51, HID52, and LYS65 (Figure 5(c)). These results indicate that BMP-2 exhibits the largest spreading and the most stable adsorption on the undegraded Mg surface, which is consistent with its highest adsorption energy shown in Figure 3. As the surface hydroxyl coverage increases during Mg degradation, the number of anchoring residues and the degree of protein spreading gradually decrease, leading to a diminished adsorption capacity of the Mg matrix for BMP-2.

Table 1. Residues in contact with the surfaces after MD simulations.

Surface	Anchoring Residues	Number of Residues
Mg	PHE51-VAL67, GLU86-ASN87	19
MgOH1	VAL25-PRO27, GLU88-VAL91	7
MgOH2	ASN51-HID52, LYS65	3
MgOH5	SER16-ASP22	7
MgOH15	ALA26-PRO28, HID9-TYR12	7

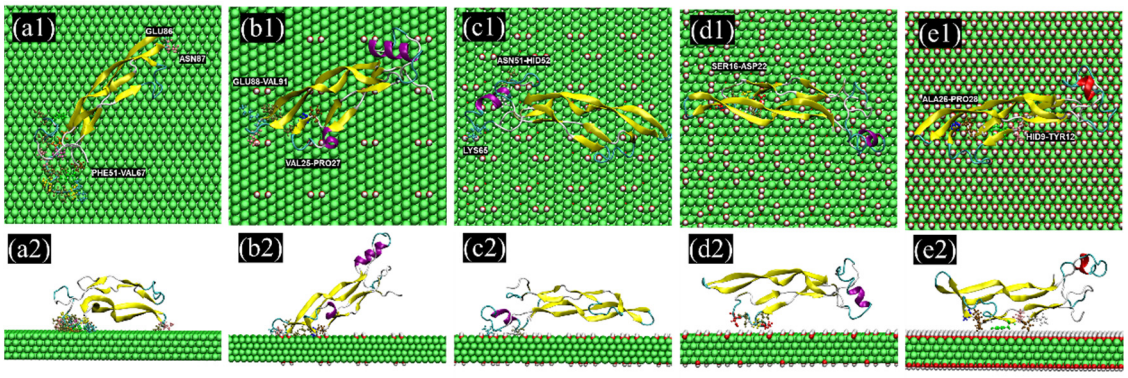

Figure 5. The adsorption configuration diagram of BMP-2 on the surfaces of (a) Mg, (b) MgOH1, (c) MgOH2, (d) MgOH5, (e) MgOH15.

BMP-2 adsorption on Mg surfaces proceeds through a multistep process: BMP-2 first diffuses toward the Mg surface, then key residues establish initial contacts with the substrate, and finally the protein displaces interfacial water molecules to achieve stable adsorption and structural rearrangement at the interface. The factors governing the adsorption strength and configuration of BMP-2 are complex; the main driving forces are van der Waals and electrostatic interactions between BMP-2 and the Mg

surface. Because of the intricate secondary structure of BMP-2 and the difficulty of probing interfacial events directly in experiments, it is challenging to identify the fundamental reasons why degradation affects protein adsorption. Consequently, to elucidate the mechanism by which Mg degradation influences BMP-2 adsorption, simplified models of both the Mg surface and BMP-2 are required for systematic analysis.

3.3. Water molecule distribution and charge distribution of Mg surfaces

In the final stage of BMP-2 adsorption on a material surface, the protein replaces and reorganizes the interfacial water layer, thereby maximizing its interaction with the surface and achieving stable adsorption and spreading [24]. When Mg undergoes degradation, the local charge on Mg atoms associated with surface hydroxyl groups increases, strengthening their interaction with surrounding water molecules. This enhanced water-surface interaction makes it more difficult for BMP-2 to displace the interfacial water layer and approach the Mg surface, ultimately hindering the adsorption and structural rearrangement of BMP-2 on degraded Mg surfaces. From the perspective of bone tissue engineering scaffold design, it is therefore desirable to preserve the integrity of the Mg surface as much as possible in order to maintain a high BMP-2 loading capacity.

In this section, the molecular mechanism governing the adsorption of the bone tissue engineering growth factor BMP-2 during pure Mg degradation was elucidated by combining molecular dynamics simulations with fluorescence protein adsorption experiments. The results indicate that degradation-induced charge redistribution at the Mg surface and the associated reorganization of the hydrated layer are the primary reasons for the weakened BMP-2 adsorption strength. Both experimental measurements and simulations consistently show that the BMP-2 adsorption capacity decreases progressively with Mg degradation. The MD simulations further reveal that BMP-2 exhibits the largest number of anchoring residues, the greatest contact area, and the smallest center-of-mass distance on the undegraded Mg surface, leading to the strongest interfacial interaction. As Mg degrades, the number of effective adsorption sites between BMP-2 and the surface decreases with increasing degradation degree, and the interaction strength is correspondingly reduced, confirming that Mg degradation inhibits BMP-2 adsorption on the surface.

4. Conclusions

By investigating the adsorption behavior of BMP-2 on pure Mg and on Mg with different degradation degrees, this study elucidated how degradation-induced surface charge redistribution affects BMP-2 adsorption. The combined results of BMP-2 adsorption experiments and molecular dynamics simulations demonstrate that, as Mg degrades, the number of effective adsorption sites between BMP-2 and the surface decreases progressively, leading to a corresponding reduction in interaction strength.

Analysis of the adsorption characteristics of representative functional groups on pure and hydroxylated Mg surfaces further shows that degradation reverses and reorganizes the interfacial hydrated layer, which mediates the decrease in adsorption strength between functional groups and the Mg surface. The rearrangement of surface charges during degradation alters the structure of the hydration layer and is identified as the main reason for the inhibited adsorption of both BMP-2 and relevant functional groups on Mg. This work, starting from the design requirements of Mg-based

metallic scaffolds for bone tissue engineering, systematically evaluates the BMP-2 loading capacity under service degradation conditions and provides a mechanistic basis for the rational feasibility design of such scaffolds.

Use of AI tools declaration

The authors declare they have not used Artificial Intelligence (AI) tools in the creation of this article.

Acknowledgments

The authors gratefully acknowledge the financial support from the National Natural Science Foundation of China (Grant No. 5250031135).

Conflict of interest

The authors declare that there is no conflict of interest.

References

1. McDermott AM, Herberg S, Mason DE, Collins JM, Pearson HB, Dawahare JH, et al. (2019) Recapitulating bone development through engineered mesenchymal condensations and mechanical cues for tissue regeneration. *Sci Transl Med* 11: eaav7756. https://doi.org/10.1126/scitranslmed.aav7756
2. Atala A, Kasper FK, Mikos AG, (2012) Engineering complex tissues. *Sci Transl Med* 4: 160rv12. https://doi.org/10.1126/scitranslmed.3004890
3. Hu X, Wang Y, Tan Y, Wang J, Liu H, Yang S, et al. (2017) A difunctional regeneration scaffold for knee repair based on aptamer-directed cell recruitment. *Adv Mater* 29: 1605235. https://doi.org/10.1002/adma.201605235
4. Chen L, Deng C, Li J, Yao Q, Chang J, Wang L, et al. (2019) 3D printing of a lithium-calcium-silicate crystal bioscaffold with dual bioactivities for osteochondral interface reconstruction. *Biomaterials* 196: 138–150. https://doi.org/10.1016/j.biomaterials.2018.04.005
5. Zhang Y, Xu J, Ruan YC, Yu MK, O'Laughlin M, Wise H, et al. (2016) Implant-derived magnesium induces local neuronal production of CGRP to improve bone-fracture healing in rats. *Nat Med* 22: 1160–1169. https://doi.org/10.1038/nm.4162
6. Grünewald TA, Rennhofer H, Hesse B, Burghammer M, Stanzl-Tschegg SE, Cotte M, et al. (2016) Magnesium from bioresorbable implants: Distribution and impact on the nano-and mineral structure of bone. *Biomaterials* 76: 250–260. https://doi.org/10.1016/j.biomaterials.2015.10.054
7. Li X, Liu X, Wu S, Yeung KWK, Zheng Y, Chu PK, (2016) Design of magnesium alloys with controllable degradation for biomedical implants: From bulk to surface. *Acta Biomater* 45: 2–30. https://doi.org/10.1016/j.actbio.2016.09.005
8. Zhao D, Witte F, Lu F, J Wang, J Li, L Qin, (2017) Current status on clinical applications of magnesium-based orthopaedic implants: A review from clinical translational perspective. *Biomaterials* 112: 287–302. https://doi.org/10.1016/j.biomaterials.2016.10.017

9. Song B, Li W, Chen Z, Fu G, Li C, Liu W, et al. (2017) Biomechanical comparison of pure magnesium interference screw and polylactic acid polymer interference screw in anterior cruciate ligament reconstruction—A cadaveric experimental study. *J Orthop Transl* 8: 32–39. https://doi.org/10.1016/j.jot.2016.09.001
10. Khademhosseini A, Langer R, (2016) A decade of progress in tissue engineering. *Nat Protocol* 11: 1775–1781. https://doi.org/10.1038/nprot.2016.123
11. Yu L, Dawson L A, Yan M, Zimmel K, Lin YL, Dolan CP, et al. (2019) BMP9 stimulates joint regeneration at digit amputation wounds in mice. *Nat Commun* 10: 1–9. https://doi.org/10.1038/s41467-018-08278-4
12. Dang M, Koh AJ, Danciu T, McCauley LK, Ma PX, (2017) Preprogrammed long-term systemic pulsatile delivery of parathyroid hormone to strengthen bone. *Adv Healthcare Mater* 6: 1600901. https://doi.org/10.1002/adhm.201600901
13. Gonzalez-Fernandez T, Tierney EG, Cunniffe GM, O'Brien FJ, Kelly DJ, (2016) Gene delivery of TGF-β3 and BMP2 in an MSC-laden alginate hydrogel for articular cartilage and endochondral bone tissue engineering. *Tissue Eng Part A* 22: 776–787. https://doi.org/10.1089/ten.tea.2015.0576
14. Schmidt-Bleek K, Willie BM, Schwabe P, Seemann P, Duda GN, (2016) BMPs in bone regeneration: Less is more effective, a paradigm-shift. *Cytokine Growth Factor Rev* 27: 141–148. https://doi.org/10.1016/j.cytogfr.2015.11.006
15. Tang D, Tare R S, Yang L Y, Williams DF, Ou KL, Oreffo ROC, (2016) Biofabrication of bone tissue: Approaches, challenges and translation for bone regeneration. *Biomaterials* 83: 363–382. https://doi.org/10.1016/j.biomaterials.2016.01.024
16. Kim SY, Kim YK, Kim KS, Lee KB, Lee MH, (2019) Enhancement of bone formation on LBL-coated Mg alloy depending on the different concentration of BMP-2. *Colloids Surf B Biointerfaces* 173: 437–446. https://doi.org/10.1016/j.colsurfb.2018.09.061
17. Zhen S, Davies GJ, (1983) Calculation of the Lennard-Jones N-M potential energy parameters for metals. *Phys Status Solidi A* 78: 595–605. https://doi.org/10.1002/pssa.2210780226
18. Huang J; Rauscher S, Nawrocki G, Ran T, Feig M, de Groot BL, et al. (2017) Charmm36m: An improved force field for folded and intrinsically disordered proteins. *Nat Methods* 14: 71–73. https://doi.org/10.1038/nmeth.4067
19. Jorgensen WL, Chandrasekhar J, Madura JD, Impey RW, Klein ML, (1983) Comparison of simple potential functions for simulating liquid water. *J Chem Phys* 79: 926–935. https://doi.org/10.1063/1.445869
20. MacKerell Jr AD, Bashford D, Bellott M, Dunbrack RL, Evanseck JD, Field MJ, (1998) All-atom empirical potential for molecular modeling and dynamics studies of proteins. *J Phys Chem B* 102: 3586–3616. https://doi.org/10.1021/jp973084f
21. Darden T, York D, Pedersen L, (1993) Particle mesh Ewald: An N log (N) method for Ewald sums in large systems. *J. Chem Phys* 98: 10089–10092. https://doi.org/10.1063/1.464397
22. Zhang YF, Wang N, Zou L, Zhang M, Chi R, (2020) Molecular dynamics simulation on the dissolution process of Kaempferol cluster. *J Mol Liq* 304: 112779. https://doi.org/10.1016/j.molliq.2020.112779
23. Bülbül E, Rupper P, Geue T, Bernard L, Heuberger M, Hegemann D, (2019) Extending the range of controlling protein adsorption via subsurface architecture. *ACS Appl Mater Interfaces* 11: 42760–42772. https://doi.org/10.1021/acsami.9b14584

24. Wang H, Yuan H, Wang J, Zhang E, Bai M, Sun Y, et al. (2021) Influence of the second phase on protein adsorption on biodegradable Mg alloys' surfaces: Comparative experimental and molecular dynamics simulation studies. *Acta Biomater* 129: 323–332. https://doi.org/10.1016/j.actbio.2021.03.063

AIMS Press